Journal of Materials Research and Technology 36 (2025) 4464–4475

Contents lists available at ScienceDirect

Journal of Materials Research and Technology

journal homepage: www.elsevier.com/locate/jmrt

Effect of polydopamine coating on the mechanical, thermal, and morphological properties of recycled PLA/kenaf fiber composites in fused deposition modelling

Sanusi Hamat [a,b], Mohamad Ridzwan Ishak [a,c,d,*], Mohd Sapuan Salit [e], Noorfaizal Yidris [a,c], Syamir Alihan Showkat Ali [b], Mohd Sabri Hussin [b]

[a] Department of Aerospace Engineering, Faculty of Engineering, Universiti Putra Malaysia, UPM Serdang, 43400, Selangor Darul Ehsan, Malaysia
[b] Faculty of Mechanical Engineering & Technology, Universiti Malaysia Perlis, Ulu Pauh, 02600, Perlis, Malaysia
[c] Aerospace Malaysia Research Centre (AMRC), Universiti Putra Malaysia, UPM Serdang, 43400, Selangor Darul Ehsan, Malaysia
[d] Laboratory of Biocomposite Technology, Institute of Tropical Forestry and Forest Products (INTROP), Universiti Putra Malaysia, UPM Serdang, 43400, Selangor Darul Ehsan, Malaysia
[e] Advanced Engineering Materials and Composites Research Centre (AEMC), Department of Mechanical and Manufacturing Engineering, Universiti Putra Malaysia, UPM Serdang, 43400, Selangor Darul Ehsan, Malaysia

ARTICLE INFO

Keywords:
FDM
3D printing
Recycled PLA
Kenaf fiber
Polydopamine

ABSTRACT

This study examines the impact of self-polymerized polydopamine (PDA) coating on the mechanical, rheological, and microstructural properties of recycled polylactic acid (rPLA)/kenaf fiber (KF) composites fabricated via Fused Deposition Modeling (FDM). Biodegradable filaments were produced by reinforcing rPLA with 5–20 wt% bast kenaf fibers and coating them with dopamine prior to melt compounding. Mechanical tests (tensile, flexural, and compression) revealed that PDA treatment substantially enhances fiber–matrix adhesion, leading to significant improvements in tensile yield stress (up to 21.92 MPa) and ultimate tensile strength (44.5 MPa), far exceeding uncoated rPLA (14.42 MPa and 18.6 MPa, respectively). Flexural strength peaked at 54.7 MPa for the 5 wt% composite, while 20 wt% kenaf markedly boosted compression strength to 65.4 MPa roughly 74 % above neat rPLA. Rheological measurements indicated that moderate fiber loadings (≤10 wt%) and PDA coating stabilize melt flow, minimizing clogging risks and supporting uniform extrusion. By contrast, higher fiber contents induced particle agglomeration and viscous instabilities, complicating FDM processability. Microscopic analyses verified that PDA-mediated bonding reduces crack propagation, despite increased porosity from higher kenaf additions. Overall, this bioinspired surface modification strategy yields sustainable rPLA-based composites with notably enhanced mechanical and favorable rheological behavior, highlighting promising applications in 3D printing and related industries.

1. Introduction

Additive Manufacturing (AM), commonly referred to as 3D printing or fused deposition modelling (FDM), has transformed various industries by enabling low-cost production of complex and customized parts from digital models. In particular, Fused Deposition Modeling (FDM), a technique that melts and deposits thermoplastic filament layer by layer has seen widespread adoption due to its affordability, straightforward maintenance, and the growing variety of compatible materials, including polylactic acid (PLA), acrylonitrile butadiene styrene (ABS), and polyethylene terephthalate glycol (PETG) [1]. Among these, PLA stands out for its biodegradability, being derived from renewable sources such as corn or sugarcane. However, the increasing concerns regarding plastic waste and climate change have prompted efforts to recycle and reuse PLA as recycled PLA (rPLA), thereby extending its lifecycle and reducing overall environmental impact [2,3]. Although rPLA retains many of the eco-friendly attributes of its virgin counterpart, repetitive thermal processing can lead to degradation, posing challenges to both mechanical performance and melt flow behavior [4]. Researchers have thus explored composite formulations that reinforce

* Corresponding author. Department of Aerospace Engineering, Faculty of Engineering, Universiti Putra Malaysia, UPM Serdang, 43400, Selangor Darul Ehsan, Malaysia.
E-mail address: mohdridzwan@upm.edu.my (M.R. Ishak).

https://doi.org/10.1016/j.jmrt.2025.04.075
Received 4 January 2025; Received in revised form 7 April 2025; Accepted 7 April 2025
Available online 8 April 2025

rPLA with natural fillers or fibers to counteract property losses and broaden application potential in 3D printing [5,6]. Incorporating natural fibers into rPLA not only boosts mechanical strength but also maintains a sustainable material profile [7]. Recent advancements in FDM have increasingly adopted natural fiber reinforcements such as kenaf, hemp, flax, and rice straw due to their sustainability, biodegradability, and ability to enhance the mechanical properties of polymer composites [8]. Among the various options, kenaf fiber (KF) has garnered attention due to its fast growth rate, low energy requirements, and favorable mechanical properties [9]. KF serve as effective nucleating agents, promoting β-phase crystal formation in PLA matrices, thereby significantly improving flexibility and impact toughness [10]. Similar nucleating and reinforcing effects have been reported for other natural fibers, including hemp [11], jute [12], and coir [13], demonstrating kenaf's competitive advantage among sustainable fibers. Jamadi et al. demonstrated that smaller kenaf fiber sizes (≤100 μm) improved tensile (45.48 MPa), flexural (64.53 MPa), and modulus (1.10 GPa) properties while also providing smoother surface finishes, attributed to superior fiber-matrix bonding and homogeneous dispersion [14]. Kenaf's fibrous structure can reinforce polymer matrices effectively, potentially resulting in enhanced strength, impact resistance, and stiffness of the final printed product [15]. Despite the potential benefits of rPLA/kenaf composites for FDM, fiber–matrix incompatibility often undermines mechanical properties. Kenaf fibers are hydrophilic and inherently difficult to disperse homogeneously in the relatively hydrophobic PLA matrix [16]. Additionally, the fibrous nature of kenaf can increase melt viscosity and introduce rheological challenges during 3D printing, such as nozzle clogging and inconsistent layer deposition [17]. These rheological challenges further highlight the necessity for optimizing fiber sizes, chemical modifications, and tailored processing parameters, as previously indicated by Khan et al., who emphasized that chemical treatments (silane, sodium acetate) significantly enhance interfacial bonding and mechanical properties, achieving tensile strengths up to 90.5 MPa and flexural strengths up to 112.5 MPa [9]. Addressing these hurdles requires careful optimization of processing parameters (e.g., extrusion temperature, speed, and fiber loading) and possibly a surface modification strategy to enhance fiber–matrix adhesion. Recently, polydopamine (PDA), formed by the self-polymerization of dopamine under mildly alkaline conditions has proven highly effective in improving interfacial bonding between different materials. Inspired by mussel adhesive proteins, PDA contains functional groups (catechols, amines) that can bind strongly with organic and inorganic surfaces, forming hydrogen or covalent bonds [18]. In the context of polymer composites, PDA coatings can bridge the interfacial gap between natural fibers and polymer matrices by boosting compatibility [19]. Supporting this, Wei et al. reported that incorporating polydopamine-modified mica in PLA significantly enhanced mechanical strength, achieving tensile strengths up to 96 MPa at 15 wt% loading, representing a 58.3 % improvement over pure PLA. Enhanced thermal stability was also noted due to improved interfacial interactions mediated by hydrogen bonding [20]. Studies on virgin PLA have shown that PDA-coated fibers enhance mechanical strength, interfacial adhesion, and even the rheological stability during melt processing [19,21]. Nonetheless, there is a knowledge gap regarding the performance of PDA-coated fibers in recycled PLA-based composites, particularly in terms of rheological properties that directly impact FDM quality and reliability. Furthermore, PDA not only improves the mechanical performance of biocomposite filaments but can also influence extrusion flow behavior, facilitating more uniform layer deposition in 3D printing [22]. Enhanced flow properties help mitigate clogging, reduce wear on the extruder, and ensure consistent filament output. Moreover, Alaa et al. highlighted that appropriate fiber treatment techniques, such as superheated steam, although reducing tensile strength due to void formation, notably improved damping properties and hydrophobicity, essential factors for reliable 3D printing [23]. This synergy between enhanced mechanical performance and improved rheological properties is crucial for rPLA-based natural fiber composites, balancing sustainability with high performance and processability. Thus, the objective of this study is to investigate the effects of polydopamine (PDA) coating on the mechanical and rheological properties of recycled PLA/kenaf fiber (rPLA/KF) composites tailored for FDM applications. In this approach, rPLA pellets were first coated with PDA and subsequently compounded with bast kenaf fibers at varying loadings (5, 10, 15, and 20 wt%) to produce filaments suitable for 3D printing. The novelty of this research lies in the formulation and application of PDA surface treatments to enhance the fiber–matrix interface and mitigate degradation issues typically associated with recycled PLA. Mechanical properties, including tensile, compression, and flexural behaviors, were characterized along with rheological analyses to evaluate flow characteristics essential for stable and reliable FDM operations. Additionally, chemical and microscopic analyses were performed to elucidate the underlying bonding mechanisms between kenaf fibers and the PDA-coated rPLA matrix, as well as to examine the microstructural effects imparted by the PDA coating. Ultimately, this research aims to advance bioinspired strategies to develop high-performance, eco-friendly composite materials suitable for diverse 3D printing applications.

2. Materials and methods

In this section, the employed manufacturing process for the fabrication of 3D Printing filament of rPLA-PDA/KF composite is outlined, along with the utilized measurement and analysis methodologies.

2.1. Materials

A commercial biodegradable recycled PLA (rPLA) (Ingeo Biopolymer 3D850) resin with specific gravity (SG) of 1.24 g/cc, peak melt temperature (PMT) of 180 °C and melt flow rate (MFR) of 9 g/10min (210 °C and 2.16 kg) developed especially for 3D Printing applications also having a faster crystallization rate and able to develop improved heat-resistance was obtained from NatureWorks, USA. A bundle processed of bast kenaf fiber having a diameter range between 50 μm and 80 μm was provided by National Kenaf and Tobacco Board (LKTN), Perlis, Malaysia. Dopamine hydrochloride (DA) (98 %), ATX Tris buffer, Sodium periodate ($NaIO_4$) and deionized (DI) water was purchased from Sigma Aldrich (Malaysia).

2.2. Preparation of rPLA-coated dopamine and granule kenaf fiber

Initially, 2 mg of dopamine hydrochloride was dissolved in a 10 mM ATX Tris buffer and stirred for 2 h until the aqueous solution reached a pH of 8.5, a condition known to facilitate the self-polymerization of dopamine into polydopamine (PDA) [21]. Next, recycled PLA (rPLA) pellets were immersed in this dopamine solution. To prevent the uncontrolled deposition of PDA nanoparticles on the pellet surfaces, the mixture was stirred continuously for 4 h. Once the coating process was complete, the rPLA pellets coated with dopamine (rPLA-PDA) (see Fig. 1 (a)) were rinsed thoroughly with deionized water, then air-dried at 80 °C for 4 h. In parallel, bast kenaf fibers were prepared by first soaking them in distilled water for 4 h to remove dust, debris, and other contaminants. The fibers were then dried in open air for approximately 8 h, followed by an additional 2 h in an air-drying oven (BOV-T50F, Biobase, Germany) at 80 °C to ensure thorough removal of moisture inside and on the surface of the fibers [4,19]. After drying, the kenaf fibers were crushed and ground into smaller fragments (<500 μm) using an Ultra Fine Automatic Powder Grinder (YF3, iPharmachine, China). To eliminate undesired larger particles that might compromise the fiber–matrix interaction, the ground kenaf fibers were subjected to a sieving process using an automatic sieve shaker (NL1015X/005, NL Scientific, Malaysia). Fig. 1(b) illustrates the resulting granule form of bast kenaf fiber, which has an average length of approximately 60 μm. These granulated fibers are better suited for blending with rPLA, as the smaller,

Fig. 1. (a) PLA pellet coated dopamine (rPLA-PDA), (b) granule bast kenaf fiber, (c) rPLA-PDA/KF20 (20 wt%) pellets.

more uniform particle size enhances fiber dispersion and interfacial bonding strength in subsequent composite processing.

2.3. Preparation of rPLA-PDA pellets blend with granule kenaf fiber (rPLA-PDA/kenaf pellet)

The recycled PLA pellets coated with polydopamine (rPLA-PDA) were first oven-dried at 80 °C for 6 h to remove residual moisture. This pre-drying step minimizes the risk of porosity or air bubbles forming during melt blending [17]. Afterward, the dried rPLA-PDA pellets and granule kenaf fibers were premixed in a WSQB-50 plastic mixer (ACC Machine, China) at 60 rpm to ensure uniform dispersion of the fibers within the polymer matrix. To investigate the effect of increasing kenaf fiber content, four different rPLA-PDA/kenaf weight ratios (5, 10, 15, and 20 wt%) were prepared. Each mixture was subsequently fed into a 20 mm twin-screw extruder (LabTech, UK) operating at a constant screw speed of 16 rpm. The temperature profile along the barrel was gradually increased from the feed to the die, following these zones (in °C): 155, 160, 165, 170, 175, 180, 180, 185, 185, and 185. During extrusion, the rPLA-PDA/kenaf composite emerged as a filament with a 3 mm diameter, which was then chopped using a pelletizer to yield 4 mm-length pellets. Fig. 1(c) illustrates the sample of final rPLA-PDA/KF20 pellet, ready for subsequent processing, such as filament re-extrusion for 3D printing evaluations. This pelletization step not only standardizes the material for downstream FDM fabrication but also helps maintain consistency in both mechanical and rheological tests.

2.4. Preparation of rPLA-PDA/kenaf filament

To produce the FDM filament from rPLA pellets coated with polydopamine (rPLA-PDA) blended with granule kenaf fiber, a desktop single-screw extrusion machine (SJ35, Robotdigg, China) was used (Fig. 2). The process aimed to form filaments with a 1.75 mm diameter, akin to commercial 3D printing filaments. Based on multiple experimental trials and guided by previous research [15,19], a stable and uniform filament was obtained by setting three extrusion temperatures (from the hopper to the filament-forming die) to 120, 175, and 180 °C, respectively, with a constant extrusion speed of 5 rpm. Before filament extrusion, the rPLA-PDA/kenaf pellets were pre-heated in an air-drying oven (BOV-T50F, Biobase, Germany) at 60 °C for 2 h to remove residual moisture. The resulting melt was then extruded through the single-screw extruder to form continuous filaments. An inline filament diameter gauge, installed at the spooler section, monitored the filament thickness every 2 m to ensure consistent diameter throughout the extrusion run. Each fabricated filament sample, representing different kenaf fiber ratios, was examined via SEM to evaluate the uniformity of fiber dispersion prior to 3D printing. Fig. 3 shows a completed 3D printing filament prepared with 5 wt% kenaf fiber (rPLA-PDA/KF5), and Fig. 4 depicts the final rPLA-PDA/Kenaf filaments at varying fiber loadings. This preliminary assessment ensured that mechanical and rheological properties would be accurately characterized in subsequent 3D printing experiments.

2.5. Fabrication of rPLA-PDA/kenaf FDM specimens

Three types of test specimens which is tensile (ASTM D638) [24],

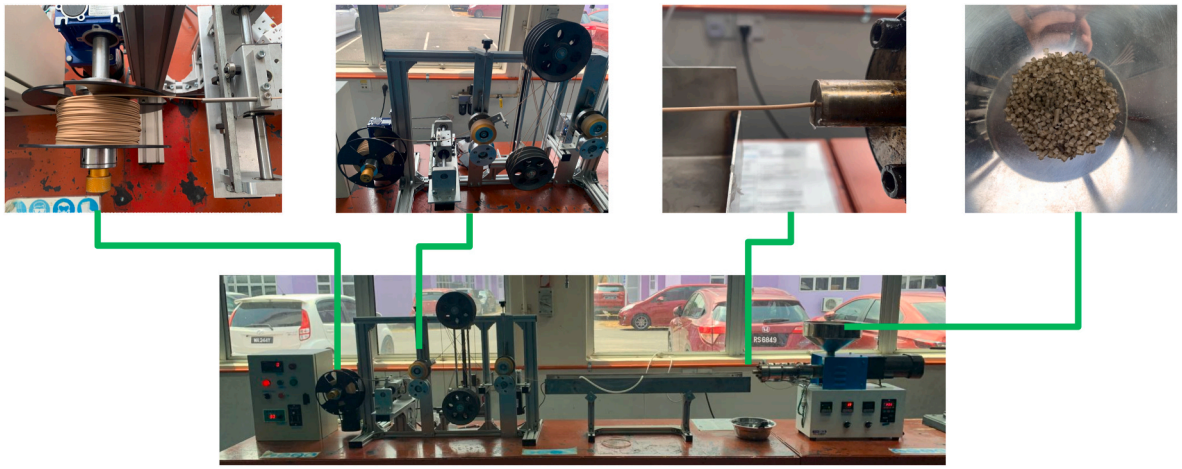

Fig. 2. Filament fabrication process of rPLA-PDA/KF.

Fig. 3. Sample of 3D Printing filament rPLA-PDA/KF5 (5 wt%) for 1.75 mm average diameter.

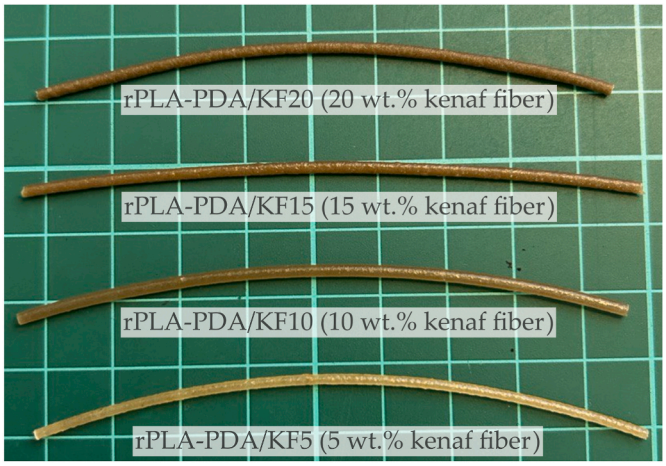

Fig. 4. Sample of 3D Printing filament rPLA-PDA/KF in different wt.% ratio.

flexural (ASTM D790) [25] and compression (ASTM D695) [26] were designed using CATIA CAD software. Each design was imported into the Qidi slicer to generate G-code files, which were subsequently printed using a Qidi X-Max 3D Printer (China). A line infill pattern set at 100 % density, with raster angles alternating at 0° and 90°, was selected to optimize load distribution and maximize part strength in accordance with previous findings [27]. Table 1 provides a summary of the key printing parameters, such as nozzle temperature, layer height, and print speed, which were used to ensure consistent fabrication. Prior to printing, the rPLA-PDA/Kenaf filaments were dried to minimize moisture-related defects, thereby reducing the likelihood of void formation during extrusion. Each specimen type was printed in batches of five to meet ASTM standard requirements, resulting in a total of 60 samples to account for the four different fiber loadings and three ASTM test standards. Fig. 5 illustrates sample specimens for tensile (ASTM D638), compression (ASTM D695), and flexural (ASTM D790) tests at 5 wt% kenaf fiber content (rPLA-PDA/KF5). The printed specimens were subsequently subjected to mechanical testing and further analyses to elucidate the influence of polydopamine coating and kenaf fiber reinforcement on the properties and performance of rPLA-based composites.

Table 1
Printing parameters (Qidi X-Max printers) for specimen fabrication.

Parameters	Value
Printing speed	40 m/s
Layer height	0.2 mm
Nozzle diameter	0.4 mm
Extruder temperature	190 °C
Bed temperature	55 °C
Infill pattern	Line
Infill density	100 %
Raster angle	0° or 90°

2.6. Characterization

This section outlines the analyses performed to assess the rPLA-based composites coated with PDA and reinforced with kenaf fibers. FTIR verifies the PDA coating and fiber–matrix interactions. A quasi-static mechanical test evaluates tensile, flexural, and compression properties of 3D-printed specimens. SEM examines fiber dispersion, interfacial adhesion, and fracture surfaces, while thermal analyses (TGA, DTG, and DSC) determine decomposition profiles, crystallization behavior, and overall thermal stability for FDM processing.

2.6.1. FTIR on rPLA-PDA coated pellets

Fourier Transform Infrared (FTIR) spectroscopy was conducted on rPLA pellets coated with polydopamine (rPLA-PDA), and rPLA-PDA/kenaf pellets to elucidate chemical bonding and confirm the presence of functional groups introduced by PDA. The samples, each less than 2 mm in diameter and 3 mm in length, were analyzed in transmission mode using a Spectrum 3 spectrometer (PerkinElmer, USA). Scans were performed in the 4000–400 cm^{-1} range with a 4 cm^{-1} resolution. To minimize experimental variability, each pellet was measured three times. Comparative analysis of these spectra helped identify the characteristic peaks associated with polydopamine and assess the potential chemical interactions between rPLA, PDA, and kenaf fibers.

2.6.2. Mechanical characterization on rPLA-PDA/kenaf FDM printed specimens

The tensile, compression, and flexural tests were conducted using the MODEL AG-X 50 kN (SHIMADZU, Japan). The dimensions of the tensile test specimen, which was based on ASTM D638, were 165 x 20 × 4 mm, with the central specimen part's width being 13 mm. A crosshead speed rate of 1 mm per minute was used to test five specimens. Fig. 6(a) depicts the 3D-printed PLA-PDA/KF5 mechanical specimen being put through a

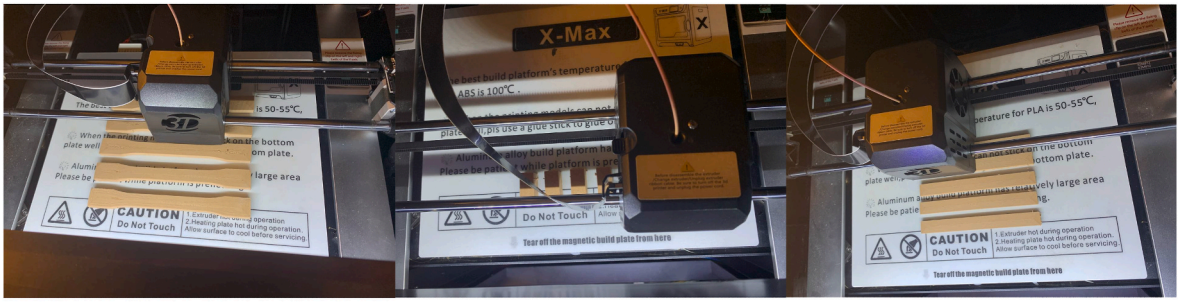

(a) (b) (c)

Fig. 5. 3D Printed specimen design of (a) ASTM D638 (Tensile), (b) ASTM D695 (Compression) and (c) ASTM D790 (Flexural) with a fiber kenaf content of 5 wt%.

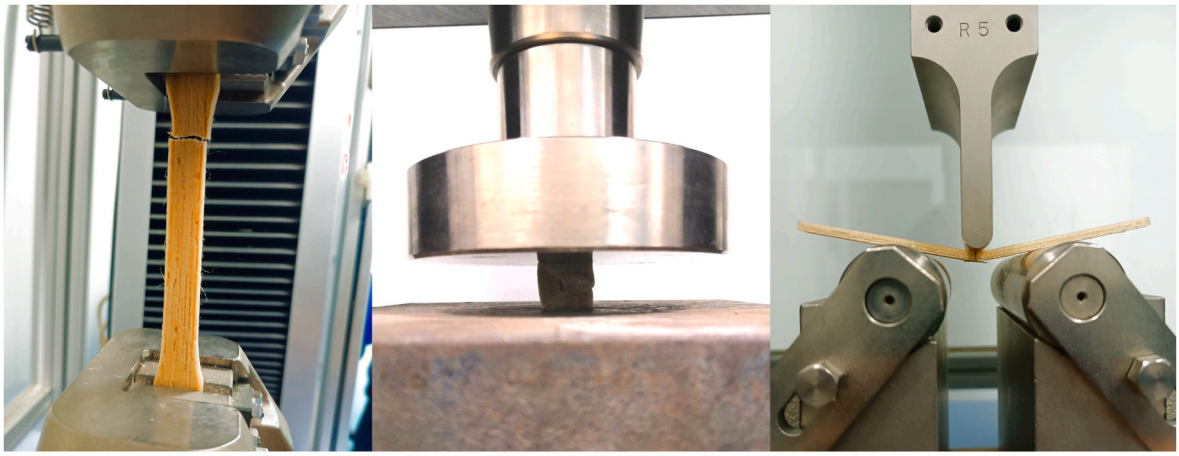

(a) (b) (c)

Fig. 6. 3D Printed specimen mechanical during the test of (a) ASTM D638 (Tensile), (b) ASTM D695 (Compression), and (c) ASTM D790 (Flexural) with a fiber kenaf content of 5 wt%.

tensile test. Fig. 6(b) shows a sample 3D-printed specimen of rPLA-PDA/KF5 mechanical during a compression test. The compression test specimen according to ASTM D695 had dimensions of 20 x 20 × 40 mm and was measured with the same tensile test crosshead speed rate of 1 mm/min for five specimens. The density of rPLA-PDA/KF in different wt.% is calculated using Equation (1).

$$\rho_c = \Sigma(wt. \times \rho)_{i+1} \tag{1}$$

where, ρ_c is the density of FDM composite filament (kg/m^3), wt. is the mass content of matrix and fiber (kg), ρ is the density of matrix and fiber (kg/m^3). The tensile and compressive strength of the FDM specimen rPLA-PDA/KF is calculated using Equation (2).

$$\sigma = \frac{F}{A} \tag{2}$$

where, σ is the tensile and compressive strength of the FDM specimen (Pa), F is the maximum force at break (N), and A is the area of the cross-section (m^2). The modulus of resilience of the FDM specimen rPLA-PDA/KF is calculated using Equation (3).

$$\mathscr{U}_r = \frac{\sigma_{el}^2}{2E} \tag{3}$$

where, $\mathscr{U}_r$ is the modulus of resilience of FDM specimen rPLA-PDA/KF (MJ/m^3), σ_{el} is the stress at the elastic limit (Pa) and E is the elastic modulus (Pa). The modulus of the toughness of the FDM specimen rPLA-PDA/KF can be found using Equation (4).

$$\mathscr{U}_t = \left(\frac{\sigma_{el} + \sigma_{uts}}{2}\right) \cdot \varepsilon_u - \left(\frac{\sigma_{el} + \sigma_{uts}}{2}\right)^2 \cdot \frac{1}{2E} \tag{4}$$

where, $\mathscr{U}_t$ is the modulus of the toughness of FDM specimen rPLA-PDA/KF (MJ/m^3), σ_{el} is the stress at the elastic limit (Pa), σ_{uts} is the ultimate tensile stress (Pa), ε_u is the ultimate strain (%) and E is the elastic modulus (Pa). As shown in Fig. 6(c), a sample 3D-printed specimen of rPLA-PDA/KF5 mechanical during a flexural test with dimensions of 80 x 20 × 5 mm underwent the test. All five specimens likewise used the identical crosshead speed rate of 1 mm/min. Every test was carried out at room temperature. The flexural strength of the FDM specimen rPLA-PDA/KF is calculated using Equation (5).

$$\sigma = \frac{3PL}{2bd^2} \tag{5}$$

where, σ is the flexural strength of the FDM specimen (Pa), P is the maximum force at break (N), L is the support span (mm), b is the width of the beam tested (mm), and d is the depth of the beam tested (mm).

2.6.3. Microstructure morphology analysis (SEM)

A scanning electron microscope (SEM, VEGA 4, Vega Compact, Tescan, USA) operating at an acceleration voltage of 10 kV was employed to examine the microstructural features of the polydopamine (PDA) coating on rPLA pellets, as well as the fracture surfaces of the tensile, compression, and flexural test specimens. Prior to SEM observation, all samples were sputter-coated with a thin layer of gold (approximately 10 nm, applied for 30 s) to enhance surface conductivity and obtain high-quality images. This preparation enabled detailed

visualization of fiber–matrix interactions, including the extent of PDA coverage on the rPLA pellets and the distribution of kenaf fibers within the composite. Special attention was given to identifying potential voids, fiber pull-out, and any evidence of enhanced fiber–matrix adhesion resulting from the PDA treatment. Fig. 7 illustrates an example SEM micrograph obtained from a 3D-printed ASTM D638 specimen containing 5 wt% kenaf fibers (rPLA-PDA/KF5), highlighting key morphological features such as fiber orientation, coating uniformity, and fracture pathways.

2.6.4. TGA, DTG and DSC on rPLA-based composites

Thermal characterization of the rPLA-based composites was conducted using thermogravimetric analysis (TGA), derivative thermogravimetry (DTG), and differential scanning calorimetry (DSC). For DSC measurements, approximately 10 – 12mg of each sample was weighed into aluminum crucibles, sealed, and then heated from 30°C to 300°C at a rate of $10°Cmin^{-1}$ under a nitrogen flow of 20 mL^{min-1}, in accordance with ASTM E1131 [28]. The DSC instrument (Mettler Toledo) was equipped with an intracooler system, maintaining an inert N_2 environment throughout the run. From the DSC thermograms, the glass transition temperature (Tg), cold crystallization temperature (Tcc), melting temperature (Tm), and melting enthalpy (ΔHm) were derived. The percentage of crystallinity ($\%X_c$) was calculated using Equation (6).

$$\%X_c = \frac{\Delta H_m}{\Delta H_m^\circ} \times 100 \tag{6}$$

where ΔH_m° is the melting enthalpy of 100% crystalline PLA ($93.1Jg^{-1}$) [16]. This crystallinity was then adjusted to reflect the actual rPLA weight fraction in each composite formulation. A PerkinElmer TGA 4000 system was employed to determine thermal degradation profiles (TGA) and to perform derivative thermogravimetry (DTG). Samples (rPLA, kenaf fibers, and rPLA/kenaf composites) of approximately 10–12mg were heated from 30°C to 500°C at a $5°Cmin^{-1}$ ramp under nitrogen at $0.2Lmin^{-1}$. The onset decomposition temperatures, maximum degradation temperatures, and residual mass were obtained from these TGA/DTG curves. By comparing the thermal events of neat rPLA, pure kenaf fibers, and the rPLA/kenaf composite blends, the influence of PDA treatment and kenaf fiber content on thermal stability and char formation could be ascertained.

3. Results and discussions

3.1. FTIR analyses on rPDA-PLA coated pellets

The FTIR spectra of rPLA pellets coated with polydopamine (rPLA-PDA) and rPLA-PDA reinforced with kenaf fibers are presented in Fig. 8. As shown, broad O–H stretching bands appear between 3300 cm^{-1} and

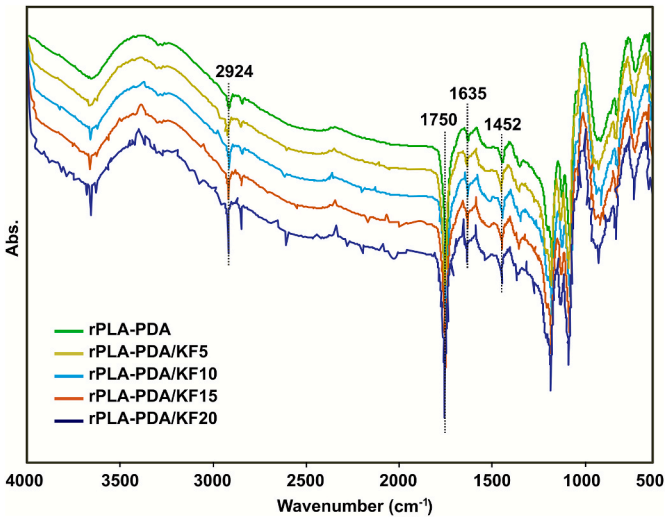

Fig. 8. FTIR spectra of dopamine coating on rPLA-based composite.

3100 cm^{-1}, indicative of polymeric hydrogen bonding [21]. A C–H stretching band at 2924 cm^{-1} corresponds to aromatic moieties in the PDA layer, while N – H bending vibrations are identified near 1635 cm^{-1}. The characteristic C = O stretching of ester groups, typically detected around 1750 cm^{-1}, and the asymmetric C–H deformation of CH_3 groups at 1452 cm^{-1} confirm the presence of the underlying rPLA matrix [18,22]. Compared to unmodified rPLA, the rPLA-PDA spectra reveal overlapping peaks near 1635 cm^{-1} often associated with C = C resonance in the PDA aromatic ring and N – H bending-alongside weaker peaks around 1410 cm^{-1}, attributable to N – H shearing vibrations [6]. These new signals confirm a robust dopamine coating on the rPLA pellets. Among the fiber-reinforced samples, rPLA-PDA/KF20 displays a notably diminished peak at $2924cm^{-1}$, suggesting that dopamine's phenolic hydroxyl and amine groups have formed strong hydrogen bonds with the free hydroxyl groups on the kenaf fibers [21]. Moreover, as kenaf content increases, the progressively decreasing peak intensity at 2924 cm^{-1} implies heightened cellulose exposure-i.e., more available fiber surface for PDA to interact with-and underscores the increased polarity of the kenaf fibers. Interestingly, the lowest characteristic peak intensity near 3415 cm^{-1} in rPLA-PDA/KF20 indicates stronger alkali-cellulose reactions, potentially leading to sodium cellulose formation and partial fiber surface breakage.

In addition, the carbonyl stretching near 1750 cm^{-1}, visible in all samples, notably vanishes or weakens upon dopamine treatment, aligning with prior findings that dopamine solutions can dissolve specific hemicellulose components in the carbonyl absorption region [19].

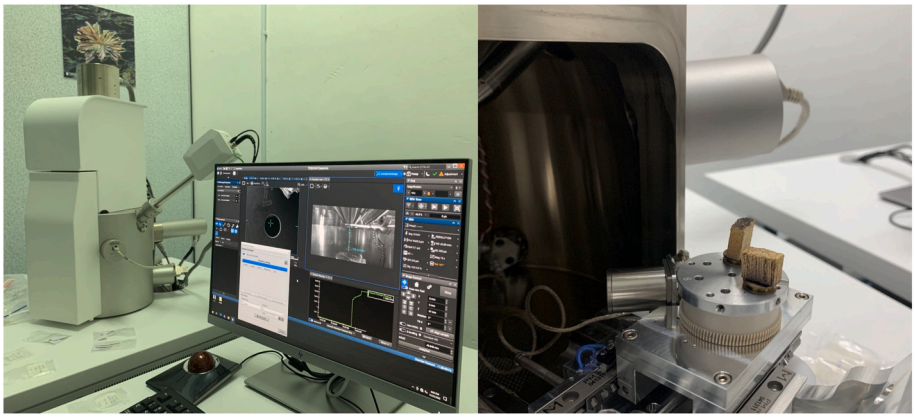

Fig. 7. Microstructure morphology analysis (SEM) for 3D Printed ASTM D638 rPLA-PDA/KF5 specimens.

This process effectively removes impurities such as wax, lignin, and hemicellulose from the kenaf fibers during blending. Consequently, by melting rPLA and dopamine at extrusion temperatures, the kenaf fibers experience in situ coating and cleaning, thereby improving the interfacial properties between fiber and polymer. Ultimately, the dopamine coating fosters more cohesive fiber-matrix bonding in rPLA-based composites, which tranclates to enhanced mechanical and thermal performance in the finished materials.

3.2. The effect of PDA coating and kenaf fiber on mechanical properties of rPLA/kenaf composites FDM printed specimens

Fig. 9(a)–. 10(a) and 11(a) present the stress–strain curves from tensile, flexural, and compression tests on recycled PLA (rPLA), rPLA coated with polydopamine (rPLA-PDA), and rPLA-PDA reinforced with kenaf fiber at four different weight percentages—5 wt.% (rPLA-PDA-KF5), 10 wt% (rPLA-PDA-KF10), 15 wt% (rPLA-PDA-KF15), and 20 wt% (rPLA-PDA-KF20). The corresponding mechanical data are summarized in Fig. 9(b)–. 10(b) and 11(b), while Tables 2 and 3 provide further insight into density, specific mechanical properties, and energy absorption parameters (e.g., modulus of resilience, modulus of toughness, fracture strain). Collectively, these results underscore how moderate kenaf fiber content (around 5 wt%) and PDA surface modification significantly improve tensile and flexural properties, whereas higher fiber loadings can dramatically boost compressive strength but somewhat diminish the tensile and flexural responses. In the tensile tests, rPLA-PDA-KF5 displays the most pronounced gain, exhibiting a tensile yield stress of 21.92 MPa and an ultimate tensile strength (UTS) of 44.5 MPa, compared with 14.42 MPa and 18.6 MPa for neat rPLA. Table 2 shows that rPLA-PDA-KF5 also attains a specific tensile yield strength roughly 36–50 % higher than rPLA, reflecting improved load transfer from matrix to fibers due to robust PDA-induced bonding and homogeneous fiber dispersion [17].

Concomitantly, its Young's modulus rises from 0.043 GPa (rPLA) to 0.113 GPa, while elongation at break increases from 1.13 % to 1.92 %. These findings confirm the dual effect of fiber reinforcement and dopamine coating enhancing both stiffness and ductility by reducing voids and fiber pull-out under tension [5]. However, Table 2 also indicates that at higher kenaf contents (≥10 wt%), tensile performance drops particularly ultimate strength due to fiber clustering and void formation, which disrupt efficient stress transfer. A parallel trend is evident in the flexural data. Although rPLA and rPLA-PDA exhibit ultimate flexural strengths of 29.3 MPa and 32.5 MPa (Table 2), rPLA-PDA-KF5 achieves 54.7 MPa with a flexural modulus of 2.64 GPa—significantly exceeding the 1.43 GPa of neat rPLA [29]. Table 3 further demonstrates that rPLA-PDA-KF5 attains a notably higher modulus of resilience (0.0026 MJ/m^3) and modulus of toughness (10.68 MJ/m^3) relative to neat rPLA (0.0007 MJ/m^3 and 1.209 MJ/m^3, respectively), underscoring this composite's capacity to absorb and dissipate energy under bending loads [30]. By contrast, as fiber loading climbs above 5 wt%, flexural strengths and toughness values begin to decline, indicative of excess fiber aggregation and insufficient fiber–matrix interfacial bonding. These observations align with the statistical analysis in Tables 2 and 3, where alphabetical indicators confirm that rPLA-PDA-KF5 outperforms higher fiber loadings in terms of flexural ductility and overall energy absorption. Interestingly, compression testing reveals a contrasting pattern. As Tables 2 and 3 do not directly report compression data, the separate compression results (Fig. 11(a) and (b)) indicate that neat rPLA, which has a yield stress of 36.2 MPa, lags behind rPLA-PDA-KF20 (63.2 MPa) by roughly 75 %. This robust response at 20 wt% kenaf likely stems from densely packed fibers under compressive load, wherein PDA-mediated infiltration reduces fiber slippage or buckling [22]. Even though the Young's modulus in compression does not rise monotonically with fiber content, the data show that the ultimate compression strength and elongation at break both improve markedly at high fiber loadings (≥10 wt%).

3.3. The effect of PDA coating and kenaf fiber on fracture surfaces of rPLA/kenaf composites FDM printed specimens

Fig. 12 presents the cross-sectional fracture surface morphologies of the 3D-printed rPLA-PDA specimens with varying kenaf fiber weight percentages. Analysis of the interfacial characteristics highlights how differing amounts of kenaf fiber reinforcement influence the mechanical performance of these composites. In Fig. 12(a), the rPLA-PDA/KF5 sample exhibits a relatively smooth fracture surface, showing minimal voids and gaps, which suggests that dopamine effectively enhances the interfacial adhesion between kenaf fibers and the rPLA matrix. Matrix fracture grooves in the bed layer are observable due to tensile loading, while Fig. 12(c) reveals staggered fibers likely resulting from flaws introduced during the fiber grinding process yet still indicating adequate fiber–matrix contact, attributable to the PDA coating. By contrast, Fig. 12(d) (rPLA-PDA/KF10) demonstrates noticeable interlayer debonding between individual printed layers, attributable to suboptimal bonding conditions during FDM and localized stress concentrations arising from voids; similar observations of debonding have been documented in prior work on printed PLA materials [5,15]. Possible contributors to these defects include void formation, bead shrinkage, and incomplete inter-bead contact, which are challenges often linked to the semi-crystalline nature of PLA [9]. Moreover, the cross-sectional image in Fig. 12(f) reveals pulled-out fiber bundles flanked by cracking lines and voids, suggesting incomplete compatibility between kenaf fibers and rPLA. Nevertheless, the matrix surface remains relatively smooth, implying that PDA-induced chemical reactions still help mitigate some of the incompatibility. A direct comparison of rPLA-PDA/KF15 (Fig. 12(i)) and rPLA-PDA/KF20 (Fig. 12(j)) confirms a higher density of micro defects namely fiber agglomeration and larger voids at higher kenaf loadings, which can be linked to the hydrophilic nature of lignocellulosic fibers clashing with the hydrophobic thermoplastic matrix, thereby exacerbating porosity and impeding uniform stress distribution.

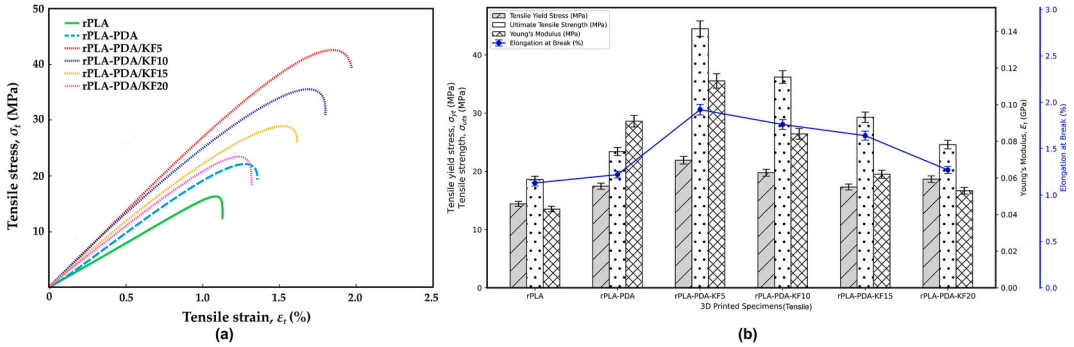

Fig. 9. (a) Tensile stress-strain curve, (b) Mechanical properties of tensile test.

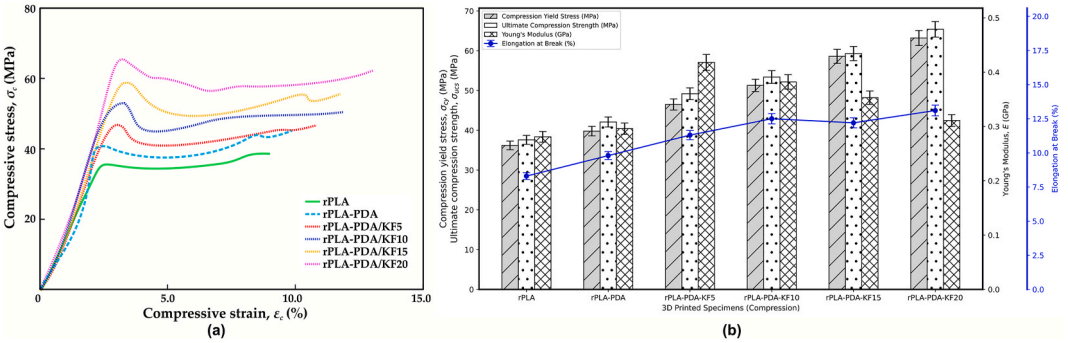

Fig. 10. (a) Compression stress-strain curve, (b) Mechanical properties of compression test.

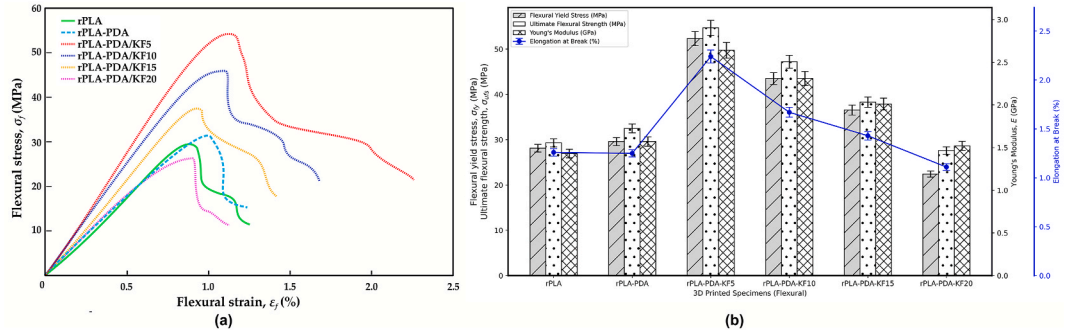

Fig. 11. (a) Flexural stress-strain curve, (b) Mechanical properties of flexural test.

Table 2
Density and tensile mechanical properties (specific modulus, specific tensile yield strength) of rPLA, rPLA-PDA, and rPLA-PDA/KF FDM composites.

Specimen	Density (kg/m^3)	Specific modulus MPa/(kg/m^3)	Specific tensile yield strength MPa/(kg/m^3)
rPLA	1240 ^{ab}	0.115 (±0.035)^{c}	0.012 (±0.028) ^{bc}
rPLA-PDA	1253^{a}	0.089 (±0.041)^{a}	0.014 (±0.033)^{b}
rPLA-rPDA/KF5	1197^{c}	1.077 (±0.032)^{b}	0.018 (±0.041)^{a}
rPLA-rPDA/KF10	1166^{c}	0.072 (±0.044)^{b}	0.017 (±0.048)^{c}
rPLA-PDA/KF15	1122 ^{cd}	0.082 (±0.052)^{c}	0.015 (±0.062)^{c}
rPLA-PDA/KF20	1079 ^{d}	0.095 (±0. 078)^{b}	0.016 (±0.088)^{d}

Table 3
Tensile mechanical properties (modulus of resilience, modulus of toughness, and fracture strain) of rPLA, rPLA-PDA, and rPLA-PDA/KF FDM composites.

Specimen	Modulus of Resilience (MJ/m^3)	Modulus of Toughness (MJ/m^3)	Fracture strain (%)
rPLA	0.0007 (±0.058)^{b}	1.209 (±0.048)^{b}	0.13 (±0.041)^{d}
rPLA-PDA	0.0014 (±0.063) ^{ab}	2.457 (±0.053) ^{ab}	0.21 (±0.046)^{c}
rPLA-PDA/KF5	0.0026 (±0.082)^{a}	10.68 (±0.073)^{a}	0.48 (±0.066)^{b}
rPLA-PDA/KF10	0.0023 (±0.087) ^{cd}	7.783 (±0.078) ^{cd}	0.43 (±0.073)^{c}
rPLA-PDA/KF15	0.0016 (±0.074)^{c}	4.688 (±0.086)^{c}	0.32 (±0.081)^{a}
rPLA-PDA/KF20	0.0017 (±0.092)^{d}	2.952 (±0.105)^{d}	0.24 (±0.109)^{c}

Note: The data in Tables 2 and Table 3 were evaluated utilizing a one-way ANOVA with a 95 % confidence threshold. Standard deviations for the test outcomes are documented within brackets, while alphabetical indicators represent statistical disparities. When groups share identical letter(s), they exhibit no substantial distinction from each other, and the opposite holds true.

Additionally, the abrupt increase in kenaf fiber surface area can exceed the available PDA coating under identical process conditions, resulting in insufficient coverage and compromised interfacial bonding [6,19]. This deficiency is further accentuated by sodium hydroxide treatment effects, where partial degradation of the kenaf structure weakens overall composite integrity. Consequently, specimens with higher kenaf loadings (e.g., 20 wt%) often show reduced mechanical properties, underscoring the importance of optimizing both fiber content and dopamine modification to enhance the fiber–matrix interface. Overall, the morphological evidence suggests that dopamine surface treatment plays a pivotal role in reinforcing kenaf fiber adhesion within recycled PLA composites, and that carefully balancing fiber content and PDA coating levels is essential for attaining superior mechanical performance in 3D-printed rPLA/PDA/kenaf systems.

3.4. Thermal analysis of rPLA-Based composites

From the TGA and DTG curves (Figs. 13 and 14) and the data in Table 4, it is evident that neat rPLA exhibits an onset degradation temperature ($T_{5\%}$) of 305.2°C, a maximum decomposition temperature (T_{max}) of 346.5°C, and a relatively low char residue of 1.26%. Introducing PDA into rPLA elevates $T_{5\%}$ to 310.4°C, indicating that the dopamine layer may provide additional thermal stability by forming stronger interfacial interactions or slight cross-linking effects at the matrix surface [31].

Meanwhile, the modest increase in char residue to 1.29% also suggests a minor protective effect, as PDA can marginally alter the decomposition pathway by generating more thermally stable residues. When kenaf fibers are incorporated (rPLA-PDA/KF), the fiber loading greatly affects both $T_{5\%}$ and the char residue. At 5 wt% fiber (rPLA-PDA/KF5), $T_{5\%}$ remains relatively high (308.3°C), but higher loadings (10 – 20wt.%) gradually lower $T_{5\%}$ and T_{max}. This drop in thermal stability is largely attributed to the lignocellulosic nature of kenaf, whose

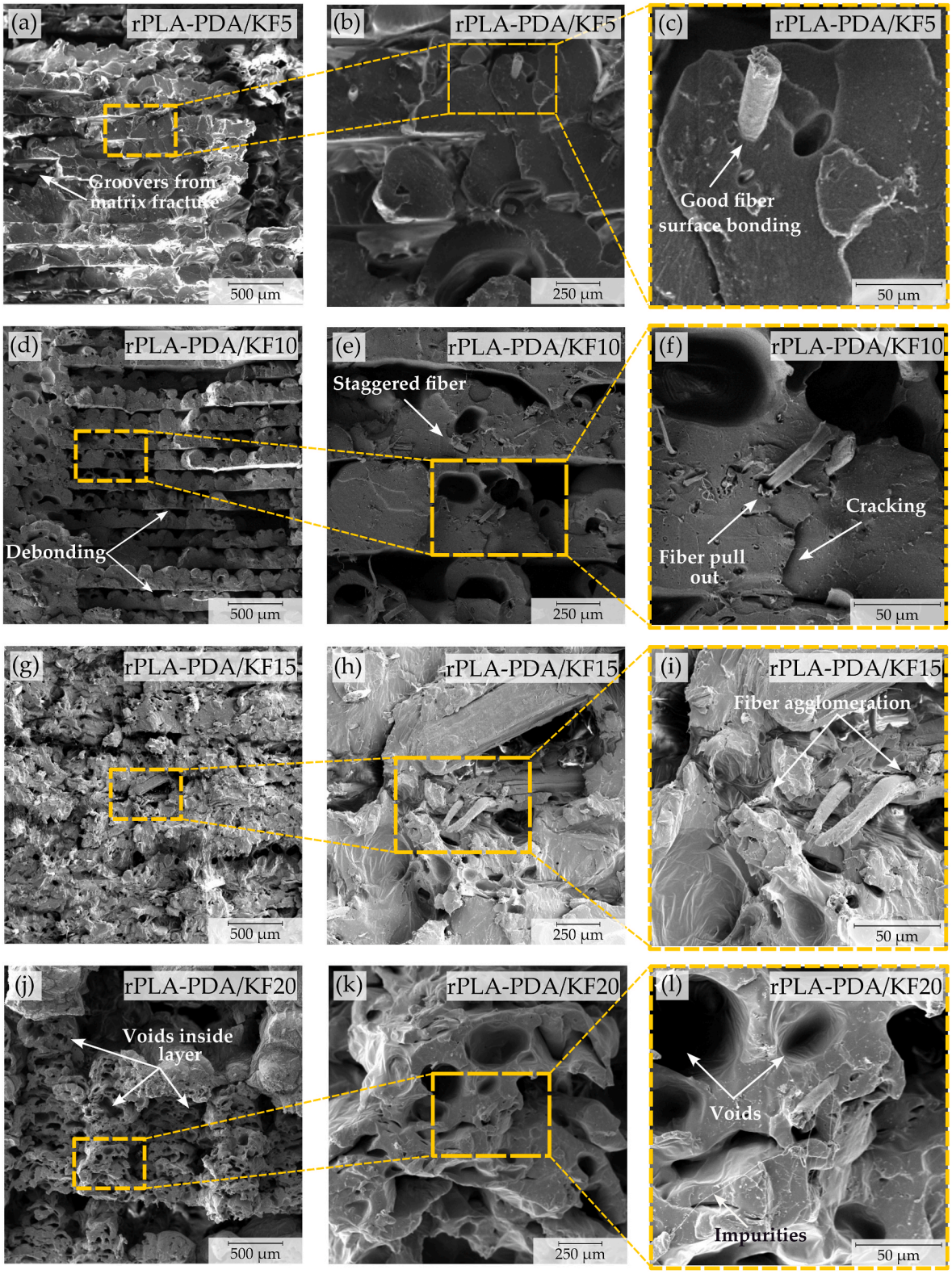

Fig. 12. SEM images of the fracture surface after tensile testing of the 3D printed rPLA-PDA/KF: (a) rPLA-PDA/KF5 (500 μm); (b) rPLA-PDA/KF5 (250 μm); (c) rPLA-PDA/KF5 (50 μm); (d) rPLA-PDA/KF10 (500 μm); (e) rPLA-PDA/KF10 (250 μm); (f) rPLA-PDA/KF10 (50 μm); (g) rPLA-PDA/KF15 (500 μm); (h) rPLA-PDA/KF15 (250 μm); (i) rPLA-PDA/KF15 (50 μm); (g) rPLA-PDA/KF20 (500 μm); (h) rPLA-PDA/KF20 (250 μm); (i) rPLA-PDA/KF20 (50 μm).

hemicellulose and lignin fractions begin degrading at slightly lower temperatures than neat PLA [17]. Nevertheless, increasing fiber content significantly raises the char residue, reaching 5.72% in rPLA-PDA/KF20, which could confer improved flame-retardant characteristics in certain applications.

Turning to the DSC thermograms (Fig. 15) and Table 5, neat rPLA shows a cold crystallization temperature (T_{cc}) at 96.92°C and a melting temperature (T_m) near 152.94°C, with a crystallinity (X_c) of 1.53%.

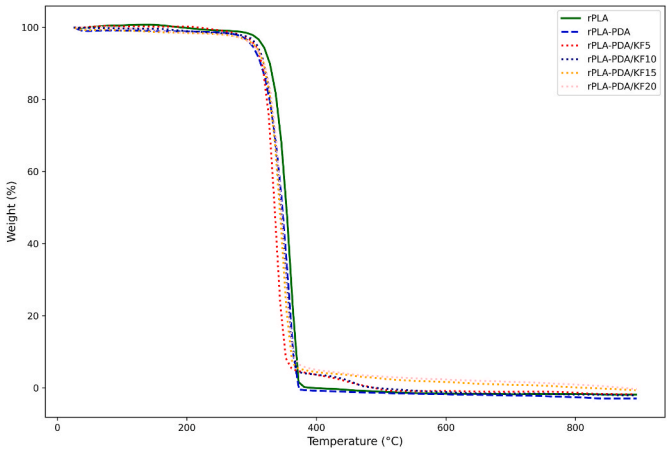

Fig. 13. TGA curves rPLA-based composites at different wt.%.

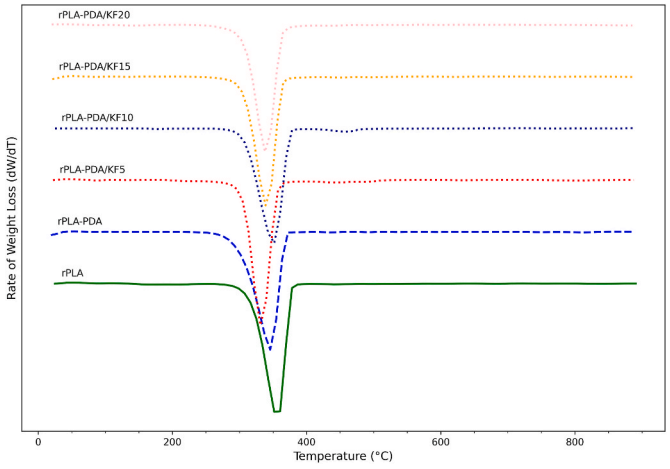

Fig. 14. DTG curves rPLA-based composites at different wt.%.

Adding PDA alone (rPLA-PDA) raises both T_{cc}(97.56°C) and T_m (153.89°C), while also enhancing crystallinity to 2.06%. This outcome implies that PDA may promote or facilitate polymer chain ordering, particularly in the more amorphous recycled PLA matrix, leading to easier nucleation and slightly greater structural organization [22,32]. The introduction of kenaf fibers further modulates crystallization: at 5 wt (rPLA-PDA/KF5), T_{cc} shifts to 98.14°C,T_m to 153.19°C, and X_c climbs to 2.86%. As fiber content increases (up to 20wt.%), both T_{cc} and T_m continue to rise, reaching maxima of 99.36°C and 154.53°C, respectively, whereas X_c can grow to 4.75 %. These trends suggest that kenaf fibers act as nucleating agents for rPLA, providing additional sites for crystal growth-especially when combined with PDA [21], which may improve fiber dispersion and fiber-matrix compatibility.

From a rheological perspective, these thermal transitions and decomposition behaviors directly influence how the molten composite flows during processing. In FDM or extrusion, higher onset degradation temperatures (~ 310°C for rPLA-PDA, ~ 308°C for rPLA-PDA/KF5) help minimize premature molecular scission, preserving melt viscosity and stability. Likewise, increased crystallinity often improves melt strength, reducing filament sag or droop, which is critical for precise layer deposition in 3D printing. Conversely, at very high kenaf contents (15-20 wt%), while crystallinity rises, partial degradation of lignocellulosic components can lead to viscous instabilities if the nozzle temperature exceeds fiber-degradation thresholds [33]. This phenomenon may cause inconsistent flow and higher risk of clogging, especially under prolonged residence times.

4. Conclusion

A biodegradable natural fiber-reinforced composite (NFRC) filament was successfully developed for fused deposition modeling (FDM) by reinforcing recycled PLA (rPLA) pellets, coated with polydopamine (PDA), with bast kenaf fibers at loadings ranging from 5 to 20 wt%. The primary findings are summarized as follows.

(i) Mechanical properties (tensile, flexural and compression):
- Optimal tensile properties were exhibited by rPLA-PDA-KF5, reaching a yield stress of 21.92 MPa and ultimate tensile strength of 44.5 MPa, surpassing neat rPLA (18.6 MPa) by over 100 %. Enhanced load transfer and improved fiber–matrix adhesion, achieved via PDA coating, contributed to these improvements.
- Flexural strength mirrored this performance, with rPLA-PDA-KF5 achieving 54.7 MPa, significantly higher than neat rPLA (29.3 MPa).
- Maximum compression strength (65.4 MPa) occurred at 20 wt % kenaf (rPLA-PDA-KF20), representing approximately a 74 % increase compared to neat rPLA. However, increased fiber

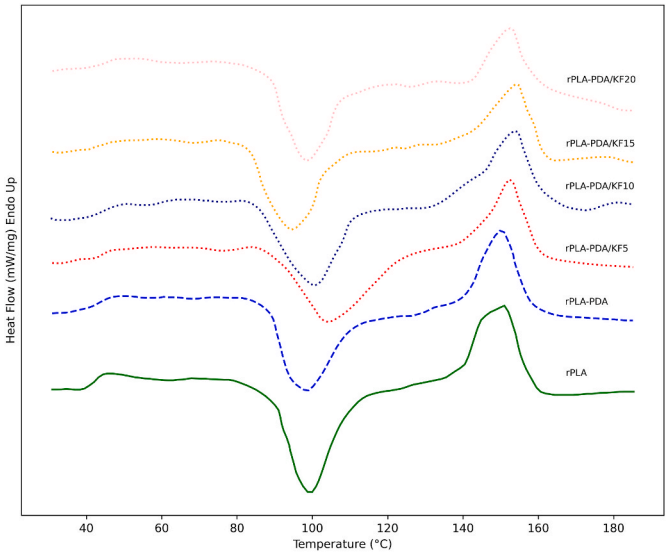

Fig. 15. DSC thermogram curves of rPLA-based composites at different wt.%.

Table 4
TGA thermal degradation temperatures analysis of rPLA-based composites.

Specimen	$T_{5\%}$(°C)	$T_{25\%}$(°C)	$T_{50\%}$(°C)	$T_{75\%}$(°C)	T_{max}(°C)	Char residue (%)
rPLA	305.2	328.5	339.1	347.9	346.5	1.26
rPLA-PDA	310.4	335.7	344.8	352.6	348.7	1.29
rPLA-PDA/KF5	308.3	327.3	337.2	346.3	346.3	1.34
rPLA-PDA/KF10	307.5	333.8	342.2	359.5	350.7	2.06
rPLA-PDA/KF15	306.0	332.0	340.7	349.4	349.4	4.92
rPLA-PDA/KF20	297.2	332.1	340.5	349.3	349.3	5.72

Table 5
DSC thermograms thermal analysis of rPLA-based composites.

Specimen	T_{cc} (°C)	ΔH_{cc} (J/g)	X_{cc} (%)	T_m (°C)	ΔH_m (J/g)	X_c (%)
rPLA	96.92	2.67	2.14	152.94	3.12	1.53
rPLA-PDA	97.56	3.21	2.57	153.89	3.85	2.06
rPLA-PDA/KF5	98.14	4.12	3.34	153.19	5.1	2.86
rPLA-PDA/KF10	98.92	5.98	4.76	154.12	7.45	3.98
rPLA-PDA/KF15	99.08	6.24	5.01	154.27	7.93	4.2
rPLA-PDA/KF20	99.36	7.1	5.89	154.53	8.35	4.75

loading introduced voids and slightly reduced tensile and flexural strengths.

(ii) Rheological Stability:
- PDA coating combined with moderate kenaf fiber loadings (≤10 wt%) improved melt-flow stability, minimized degradation, and facilitated uniform filament extrusion.
- Higher fiber contents (≥15 wt%) led to fiber agglomeration and increased viscosity-related instabilities, complicating consistent FDM processing.

(iii) Thermal Stability (TGA/DTG/DSC Analysis):
- PDA coating enhanced thermal stability by increasing the onset degradation temperature from 305.2 °C (neat rPLA) to 310.4 °C and slightly elevating char residue from 1.26 % to 1.29 %.
- Kenaf fiber incorporation significantly raised char residue to 5.72 % at 20 wt% and increased the cold crystallization temperature (T_{cc}) from 96.92 °C to 99.36 °C, indicating the nucleating influence of kenaf fibers.

The composition rPLA-PDA-KF5 demonstrated the most balanced set of tensile, flexural, rheological, and thermal properties, making it particularly suitable for general load-bearing applications. Conversely, compositions containing higher fiber loadings (≥15 wt%) showed superior performance specifically under compression, although these formulations faced greater challenges related to rheological processing. Overall, PDA-coated rPLA/kenaf fiber composites possess significant potential as sustainable, high-performance filaments suitable for various additive manufacturing applications.

Declaration of competing interest

The authors declare the following financial interests/personal relationships which may be considered as potential competing interests: Sanusi Hamat reports financial support was provided by Malaysia Ministry of Higher Education. If there are other authors, they declare that they have no known competing financial interests or personal relationships that could have appeared to influence the work reported in this paper.

Acknowledgments

The authors wish to express deepest gratitude to the Faculty of Mechanical Engineering & Technology at Universiti Malaysia Perlis (UniMAP), the Department of Aerospace Engineering at Universiti Putra Malaysia (UPM), and the Institute of Tropical Forestry and Forest Products (INTROP) for their unwavering support and for providing access to world-class laboratories and cutting-edge research facilities. This paper's publication was funded by UPM Incentive Journal Publication 2025. The authors are also profoundly grateful to the National Kenaf and Tobacco Board (LKTN) of Perlis for their invaluable contribution in supplying the high-quality kenaf fibers that were essential to this study.

References

[1] Thohid Rayhan M, et al. Advances in additive manufacturing of nanocomposite materials fabrications and applications. Eur Polym J 2024;220(August):113406. https://doi.org/10.1016/j.eurpolymj.2024.113406.

[2] Hasan MR, Davies IJ, Pramanik A, John M, Biswas WK. Potential of recycled PLA in 3D printing: a review. Sustain. Manuf. Serv. Econ. 2024;3(March):100020. https://doi.org/10.1016/j.smse.2024.100020.

[3] Olawumi MA, Oladapo BI, Olugbade TO. Evaluating the impact of recycling on polymer of 3D printing for energy and material sustainability. Resour Conserv Recycl 2024;209(June):107769. https://doi.org/10.1016/j.resconrec.2024.107769.

[4] Atiqah Abdul Azam F, Tharazi I, Bakar Sulong A, Che Omar R, Muhamad N. Mechanical durability and degradation characteristics of long kenaf-reinforced PLA composites fabricated using an eco-friendly method. Eng. Sci. Technol. an Int. J. 2024;57(August). https://doi.org/10.1016/j.jestch.2024.101820.

[5] Atakok G, Kam M, Koc HB. Tensile, three-point bending and impact strength of 3D printed parts using PLA and recycled PLA filaments: a statistical investigation. J Mater Res Technol 2022;18:1542–54. https://doi.org/10.1016/j.jmrt.2022.03.013.

[6] Kumar S, et al. Optimization of chemical treatment process parameters for enhancement of mechanical properties of Kenaf fiber-reinforced polylactic acid composites: a comparative study of mechanical, morphological and microstructural analysis. J Mater Res Technol 2023;26:8366–87. https://doi.org/10.1016/j.jmrt.2023.09.157.

[7] Khan A, Sapuan SM, Zainudin ES, Zuhri MYM. Physical, mechanical and thermal properties of novel bamboo/kenaf fiber-reinforced polylactic acid (PLA) hybrid composites. Compos Commun 2024;51(September). https://doi.org/10.1016/j.coco.2024.102103.

[8] Nazir MH, Al-Marzouqi AH, Ahmed W, Zaneldin E. The potential of adopting natural fibers reinforcements for fused deposition modeling: characterization and implications. Heliyon 2023;9(4):e15023. https://doi.org/10.1016/j.heliyon.2023.e15023.

[9] Khan A, Sapuan SM, Siddiqui VU, Zainudin ES, Zuhri MYM, Harussani MM. A review of recent developments in kenaf fiber/polylactic acid composites research. Int J Biol Macromol 2023;253(P5):127119. https://doi.org/10.1016/j.ijbiomac.2023.127119.

[10] Huy TA, Adhikari R, Lüpke T, Henning S, Michler GH. Molecular deformation mechanisms of isotactic polypropylene in α- and β-crystal forms by FTIR spectroscopy. J Polym Sci Part B Polym Phys Dec. 2004;42(24):4478–88. https://doi.org/10.1002/POLB.20117.

[11] Aliotta L, Gigante V, Coltelli MB, Cinelli P, Lazzeri A, Seggiani M. Thermo-mechanical properties of PLA/short flax fiber biocomposites. Appl. Sci. 2019;9:3797. https://doi.org/10.3390/APP9183797. vol. 9, no. 18, p. 3797, Sep. 2019.

[12] Tanaka K, Katsura T, Shinohara M, Morita Y, Katayama T, Uno K. Heat-resistant and mechanical property of jute continuous fiber reinforced PLA. J. Soc. Mater. Sci. Japan Jul. 2010;59(7):546–52. https://doi.org/10.2472/JSMS.59.546.

[13] Dong Y, Ghataura A, Takagi H, Haroosh HJ, Nakagaito AN, Lau KT. Polylactic acid (PLA) biocomposites reinforced with coir fibres: evaluation of mechanical performance and multifunctional properties. Compos. Part A Appl Sci Manuf Aug. 2014;63:76–84. https://doi.org/10.1016/J.COMPOSITESA.2014.04.003.

[14] Jamadi AH, Razali N, Malingam SD, Taha MM. Effect of fibre size on mechanical properties and surface roughness of PLA composites by using fused deposition modelling (FDM). J. Renew. Mater. 2023;11(8):3261–76. https://doi.org/10.32604/jrm.2023.028280.

[15] Lau HY, Hussin MS, Hamat S, AbdulManan MS, Ibrahim M, Zakaria H. Effect of kenaf fiber loading on the tensile properties of 3D printing PLA filament. Mater Today Proc 2023. https://doi.org/10.1016/j.matpr.2023.03.015.

[16] Tawakkal ISMA, Cran MJ, Bigger SW. Effect of kenaf fibre loading and thymol concentration on the mechanical and thermal properties of PLA/kenaf/thymol composites. Ind Crops Prod 2014;61:74–83. https://doi.org/10.1016/j.indcrop.2014.06.032.

[17] Abu Hassan NA, Ahmad S, Chen RS, Shahdan D, Mohamad Kassim MH. Tailoring lightweight, mechanical and thermal performance of PLA/recycled HDPE biocomposite foams reinforced with kenaf fibre. Ind Crops Prod 2023;197(December 2022):116632. https://doi.org/10.1016/j.indcrop.2023.116632.

[18] Xu W, Lv Y, Kong M, Huang Y, Yang Q, Li G. In-situ polymerization of eco-friendly waterborne polyurethane/polydopamine-coated graphene oxide composites towards enhanced mechanical properties and UV resistance. J Clean Prod 2022;373(April):133942. https://doi.org/10.1016/j.jclepro.2022.133942.

[19] Hamat S, et al. The effects of self-polymerized polydopamine coating on mechanical properties of polylactic acid (PLA)–Kenaf fiber (KF) in fused deposition modeling (FDM). Polymers May 2023;15(11):2525. https://doi.org/10.3390/polym15112525.

[20] yue Wei X, Li W, Li J, ting Niu X. Mussel-inspired polydopamine modified mica with enhanced mechanical strength and thermal performance of poly(lactic acid) coating. Int J Biol Macromol 2024;273(P2):133148. https://doi.org/10.1016/j.ijbiomac.2024.133148.

[21] Zhao XG, Hwang KJ, Lee D, Kim T, Kim N. Enhanced mechanical properties of self-polymerized polydopamine-coated recycled PLA filament used in 3D printing. Appl Surf Sci 2018;441:381–7. https://doi.org/10.1016/j.apsusc.2018.01.257.
[22] George E, Manoli A, P PV, Vahabi H, George SC, Anas S. Polydopamine modified polymeric carbon nitride nanosheet based ABS nanocomposites for better thermal, frictional and mechanical performance. Nano-Structures and Nano-Objects 2023; 35:100987. https://doi.org/10.1016/j.nanoso.2023.100987.
[23] Alaa M, et al. Fundamental study and modification of Kenaf fiber reinforced polylactic acid bio-composite for 3D printing filaments. Mater Today Proc 2023. https://doi.org/10.1016/j.matpr.2023.03.328.
[24] American Society for Testing and Materials. ASTM D638-14, standard practice for preparation of metallographic specimens. ASTM Int 2016;82(C):1–15. https://doi.org/10.1520/D0638-14.1.
[25] ASTM D790-17. Standard test methods for flexural properties of unreinforced and reinforced plastics and electrical insulating materials. D790. Annu. B. ASTM Stand. 2002;i:1–12. https://doi.org/10.1520/D0790-17.2.
[26] American Society for Testing and Materials International. Standard test method for compressive properties of rigid plastics D695. ASTM Int. 2002;8:1–7. https://doi.org/10.1520/D0695-15.2. April 2003.
[27] Martín MJ, Auñón JA, Martín F. Influence of infill pattern on mechanical behavior of polymeric and composites specimens manufactured using fused filament fabrication technology. Polymers 2021;13(17). https://doi.org/10.3390/polym13172934.
[28] Method ST. iTeh standards iTeh standards document Preview, vol. 8; 2000. p. 3–4. https://doi.org/10.1520/C1709-18. Reapproved 1989.
[29] Hong JH, Yu T, Park SJ, Kim YH. Repetitive recycling of 3D printing PLA filament as renewable resources on mechanical and thermal loads. Int J Mod Phys B 2020; 34(22–24):1–5. https://doi.org/10.1142/S0217979220401475.
[30] Lee D, Lee Y, Kim I, Hwang K, Kim N. Thermal and mechanical degradation of recycled polylactic acid filaments for three-dimensional printing applications. Polymers 2022;14(24). https://doi.org/10.3390/polym14245385.
[31] Xiang S, Feng L, Bian X, Li G, Chen X. Evaluation of PLA content in PLA/PBAT blends using TGA. Polym Test 2020;81(November 2019):106211. https://doi.org/10.1016/j.polymertesting.2019.106211.
[32] Arjmandi R, Ismail A, Hassan A, Abu Bakar A. Effects of ammonium polyphosphate content on mechanical, thermal and flammability properties of kenaf/polypropylene and rice husk/polypropylene composites. Constr Build Mater 2017; 152:484–93. https://doi.org/10.1016/j.conbuildmat.2017.07.052.
[33] Saleh M, Anwar S, AlFaify AY, Al-Ahmari AM, Abd Elgawad AEE. Development of PLA/recycled-desized carbon fiber composites for 3D printing: thermal, mechanical, and morphological analyses. J Mater Res Technol 2024;29(January 2024):2768–80. https://doi.org/10.1016/j.jmrt.2024.01.267.